Current-Dependent Dynamics of Bidirectional Self-Folding for Multi-Layer Polymers Using Local Resistive Heating

Moataz Elsisy
Department of Industrial Engineering,
University of Pittsburgh,
Pittsburgh, PA 15261
e-mail: MME41@pitt.edu

Evan Poska
Department of Industrial Engineering,
University of Pittsburgh,
Pittsburgh, PA 15261
e-mail: poska.2@osu.edu

Moataz Abdulhafez
Department of Industrial Engineering,
University of Pittsburgh,
Pittsburgh, PA 15261
e-mail: MMA89@pitt.edu

Mostafa Bedewy[1]
Department of Industrial Engineering,
Department of Chemical and Petroleum Engineering,
Department of Mechanical Engineering and Materials Science,
University of Pittsburgh,
Pittsburgh, PA 15261
e-mail: mbedewy@pitt.edu

The purpose of this paper is to characterize the dynamics and direction of self-folding of pre-strained polystyrene (PSPS) and non-pre-strained styrene (NPS), which results from local shrinkage using a new process of directed self-folding of polymer sheets based on a resistively heated ribbon that is in contact with the sheets. A temperature gradient across the thickness of this shape memory polymer (SMP) sheet induces folding along the line of contact with the heating ribbon. Varying the electric current changes the degree of folding and the extent of local material flow. This method can be used to create practical three-dimensional (3D) structures. Sheets of PSPS and NPS were cut to 10 × 20 mm samples, and their folding angles were plotted with respect to time, as obtained from in situ videography. In addition, the use of polyimide tape (Kapton) was investigated for controlling the direction of self-folding. Results show that folding happens on the opposite side of the sample with respect to the tape, regardless of which side the heating ribbon is on, or whether gravity is opposing the folding direction. The results are quantitatively explained using a viscoelastic finite element model capable of describing bidirectional folds arising from the interplay between viscoelastic relaxation and strain mismatch between polystyrene and polyimide. Given the tunability of fold times and the extent of local material flow, resistive-heat-assisted folding is a promising approach for manufacturing complex 3D lightweight structures by origami engineering. [DOI: 10.1115/1.4049588]

Keywords: materials processing, mechanical behavior, shape memory polymers, viscoelastic relaxation, finite element modeling, origami

1 Introduction

Origami-based approaches of fabrication have emerged as an attractive new approach to manufacturing complex three-dimensional (3D) polymer structures, wherein directed self-folding at desired locations leads to the gradual transformation of two-dimensional (2D) sheets into desired 3D structures [1–5]. In particular, leveraging viscoelastic relaxation in pre-strained polymer sheets is a promising approach for scalable origami-based manufacturing. For example, a temperature gradient across the thickness of a pre-strained polystyrene (PSPS) sheet, which is a shape memory polymer (SMP), causes the hotter side to shrink more than the cooler side. When concentrated along a line, the heat causes folds about that line, as shown in Fig. 1. This underlies the potential of using origami engineering of SMPs for manufacturing functional components made of commodity polymers such as polystyrene.

Self-folding refers to the out of plane rotation around a line that seemingly acts as a hinge on the substrate without direct mechanical loading [6,7]. This phenomenon is promising for actuation, packaging, and assembly of products. Hence, self-folding has been used for reconfigurable devices [8,9], biomedical application [10,11], solar cells [12,13], in addition to robotic actuators and sensors [14]. Recent work on self-folding has employed different stimuli, including magnets [15,16], pneumatics [17,18] swelling [19], and heat [20,21]. This paper focuses on using localized heating stimulation in order to induce self-folding in SMP based on thermomechanical viscoelastic behavior.

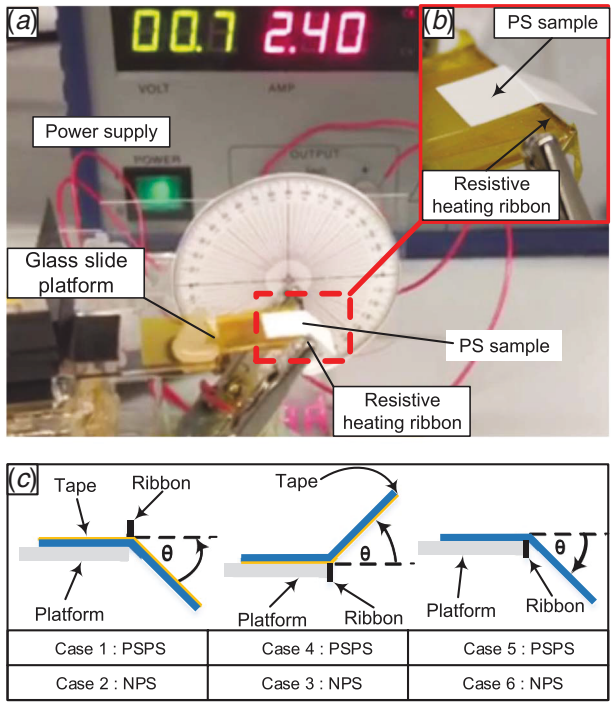

Fig. 1 Experimental setup for self-folding SMP sheets activated by the resistive heating ribbon: (*a*) photo of the experimental setup, (*b*) zoomed-in image for the contact between ribbon and polymer, and (*c*) schematic of experimental cases

[1]Corresponding author.

Contributed by the Materials Division of ASME for publication in the Journal of Engineering Materials and Technology. Manuscript received August 19, 2020; final manuscript received December 10, 2020; published online February 3, 2021. Assoc. Editor: Francis Aviles.

Non-shape memory polymers (non-SMP) and SMP have been explored for the purpose of self-folding in the literature. Uniform heating [22], laser [23], and surface tension [24] were used for self-folding of the non-SMP. Also, for self-folding of SMP, researchers have investigated different stimuli including intense light [25,26], microwave [27], resistive heating [28,29], uniform heating [30,31], and laser [32,33]. These techniques primarily differ in the underlying mechanism and dynamics of locally delivering the energy needed to drive folding. Some of the techniques depend on heat conduction through contact to deliver the energy, while others drive the self-folding through radiation/microwave heating. The main disadvantage with noncontact techniques is the difficulty of programming sequential folds since the light and microwaves will need to be focused on the desired lines, which becomes more challenging with increasing number of folding. Contact techniques, while more involved to set up, can be easily designed to allow sequential folds that enable more complex designs. Despite the number of previous reports, a comprehensive understanding of how to tune the process parameters for viable manufacturing based on bidirectional folding is still largely missing, especially with regards to independently controlling the direction, speed, and quality of folds. Hence, the purpose of this paper is to characterize the dynamics and direction of folding pre-strained polystyrene and non-pre-strained styrene (NPS) due to local contact-based heating using a custom-built setup with in situ videography. The heating is produced by forcing an electric current through the resistively heated metal ribbon in direct contact with the polymer substrate. Different configurations were used for the polymer substrates to study the effect of combining the polymer layer with polyimide (PI) tape. Polyimide was chosen because of its temperature resistance in the range of temperatures of our experiments (less than 150 °C). Also, different setups of heating were investigated to show the effect of directionality in heat propagation through the polymer layer and polyimide layer.

Results show that electric current and use of the polyimide layer can effectively control folding speed, angle, and direction, enabling the creation of complex 3D shapes based on bidirectional folding. Hence, such an approach of folding 2D substrates to 3D shapes represents a promising manufacturing route for lightweight structures and compliant mechanisms.

2 Experimental

2.1 Methods. Direct Current Power Supply (B&K Precision) with single output and range of 0–18 V was used, which allows current-controlled mode with precision 0.01 Amperes (A). The resistive heating ribbon Kanthal A-1 (Temco NCRR-23-100 Ni80/Cr20 500 × 100 μm 30.18 Ω/m @ 20 °C) was used. The temperature of the ribbon is measured at different spots between electrical terminals using a data logger (OMEGA HHM-EX540 Multimeter/Data Logger with Wireless PC Interface) along with K-type thermocouple. A commercial microscope with digital camera (Celestron) was used for real-time monitoring of the folding process.

2.2 Materials. White pre-strained polystyrene was used for all of the PSPS tests. 0.3-mm-thick commercially available sheets of shrink films (Grafix® White) were used, which bi-axially contract by 55% when heated above the glass temperature. Similar sheets were used in previous work for self-folding using different stimuli [20–28]. Plastruct (thickness 0.254 mm) styrene was used for all of the NPS control tests. All samples were cut to 10 × 20 mm using the cutter and ruler.

2.3 Setup. For the experimental setup, shown in Fig. 1, a glass slide was used as a robust platform supporting the polymer sheet while ensuring minimum heat loss due to PS contact with the insulating platform. Adhesive tape was used to hold the substrate over about 8 mm of the polymer sheet while keeping the other half of the sample overhung at the end, as shown in Fig. 1. The tape uses silicone adhesive that has an operating temperature range between −60 °C and 200 °C. To ensure uniform and repeatable pressure on the PS, the resistive ribbon was securely clamped in alligator clips. The resistive ribbon was allowed 1 min for heating up to reach steady-state temperature to eliminate the effects of initial transient heating phase before bringing the substrate and the heating ribbon in contact.

Videos of the experiments were recorded at a resolution of either 720 pixels or 1080 pixels, and rates of either 30 frames per second (fps) or 60 fps with a protractor behind the folding to measure the angle with time. A microscope video camera focused on the hinge during folding recorded at 7 fps, the heat effect on the material with time. The recording was stopped after either reaching 90 deg or after 600 s of substrate-ribbon contact. Angles were plotted with respect to time at intervals of 1–10 s, depending on the speed of folding. From several experiments, it is concluded that the best time interval that would allow us to adequately capture the dynamics is different depending on the stage of folding, as follows: 1 s interval from start time to 30 s, 3 s interval from 30 s to 60 s, 5 s interval from 60 s to 100 s, and 10 s interval from 100 s to 600 s. The angles were recorded manually by reviewing videos associated with each experiment.

Initial tests using resistive round heating wires were not as effective as the flat ribbon heated on the edge or flat side. The best results were obtained using the sharp ribbon edge, which is what will be reported on in this paper. Using the datasheet of the resistive ribbon, the expected ribbon temperature was calculated for different currents. Current value of 2.2, 2.4, 2.6, 2.8, and 3 A were chosen to achieve a temperature range of about 30 °C around glass temperature (103 °C) of polystyrene. The temperature was measured using a thermocouple directly in contact with the heating ribbon, and the experimentally obtained temperature–current calibration is shown in Table 1.

2.4 Finite Element Model. To gain qualitative insight into the bidirectional folding phenomenon, we develop a 3D finite element model (FEM) of the PSPS and polyimide on PSPS cases. ANSYS APDL was used to run the model with SOLID227 elements, which can couple the thermal and mechanical fields and handle material non-linearity like viscoelasticity, hence can be used to model this problem [34]. We utilize the material parameters used in previous simulation efforts [35,36], which use a generalized Maxwell model and the Williams–Landel–Ferry equation to account for viscoelastic effects and temperature dependence as shown in Tables 2–4. We use two models, the first being a single layer of PSPS which is modeled as an elastic–viscoelastic material and the second model is a similar layer of PSPS and a layer of Kapton polyimide (thickness 0.05 mm). The polystyrene sheet initial geometry has a

Table 1 Resistive wire temperature at each current

Current (A)	2.20	2.40	2.60	2.80	3.00
Temperature (°C)	89.75	101.15	113.05	124.25	137.45

Table 2 PS material properties

PS WLF C1	17.44
PS WLF C2	51.6 K
PS glass transition temp.	103 °C
PS Young's modulus	1.78×10^9 Pa
PS specific heat	1300 J/(kg K)
PS Poisson's ratio	0.33
PS thermal conductivity	0.14 W/(m K)
PS density	1050 kg/m^3

Table 3 Kapton material properties

Kapton Young's modulus	2.5×10^9 Pa
Kapton density	1420 kg/m^3
Kapton Poisson's ratio	0.33
Kapton specific heat	1090 J/(kg K)
Kapton thermal conductivity	0.12 W/(m K)

Table 4 Prony coefficients for the viscoelastic PS model

Branch no.	1	2	3	4	5	6
$g\ (i)$	0.2089	0.3654	0.3037	0.1011	0.01243	0.004661
$\tau\ (i)$ (s)	1.182	14.77	114.8	402	3096	25,680

length of 2.5 mm, a width of 1.25 mm, and a thickness of 0.2 mm. The problem is divided into two parts, the first being a thermal programming step to develop the pre-strain and the second being a local heating step to induce the folding as illustrated in Fig. 2(*a*). In the thermal programming step, volumetric heating ($Q_{gen} = 0.25$ W/mm^3, 0.45 s) is applied to the entire geometry, heating it up to a temperature higher than the PS glass transition temperature T_g. Convection boundary conditions are active at the sheet boundaries ($h = 5\times10^{-6}$ W/(mm^2 °C), $T_\infty = 22$ °C). After the heating is completed and the sheet temperature exceeds the T_g, a pressure P is applied to the upper sheet surface and ramped to a value of 2.4 MPa in 10 s, compressing the sheet, and then the load is held constant. The sheet dimensions after compression had a length of 2.92 mm, a width of 1.46 mm, and a thickness of 0.146 mm. While the pressure is held constant, negative volumetric heating ($Q_{gen} = -0.15$ W/mm^3, 0.45 s) is applied to cool the sheet to below the T_g, hence maintaining the pre-strained state. The model is then heated at the lower surface center (width = 0.2 mm) using a constant heat flux ($Q_{surf} = 7.5\times10^{-2}$ W/mm^2, 0.25 s) to drive the folding. We monitor the temperature, axial strain, and folding angle across the center of the sheet for both cases during the heating process. Tetrahedral elements are used to mesh the geometry as shown in Fig. 2(*b*) with a total element number of 14,000 elements. The element number is decided using a convergence study as illustrated in Fig. 2(*c*). In the two-layer case, the polyimide elements were integrated with the pre-strained layer through element birth of the lower polyimide layer with the start of the second load step. The two layers are bonded together.

3 Experimental Results

Six cases for different configurations of heating and the two polymer layers were used in the experiments as shown in Fig. 1(*c*). In cases 1 and 2, the *top* tape-covered side of the substrate was heated by the *bottom* tip of the heating ribbon. PSPS was used for case 1; however, NPS was used in case 2. For cases 3 and 4, the same was done except that the *bottom* tape-covered side was heated using the *upper* tip of the heating ribbon. Finally, for cases 5 and 6, the polymer was heated without any tape using the *upper* tip of the ribbon, where PSPS was used in case 5, and NPS for case 6.

3.1 Case 1. In this case, a substrate consists of a layer of Kapton polyimide tape that is adhered to the PSPS sheet, and the substrate is heated with the bottom tip of the resistive ribbon. The results of substrate folding are shown in Fig. 3. The schematic drawing of substrate folding is presented in Fig. 3(*a*). Results of folding angle as a function of time are shown in Figs. 2(*b*)–2(*e*) for currents 3 A, 2.8 A, 2.4 A, and 2.2 A, respectively. The average of multiple experimental measurements for fold angle is plotted, and these averages are compared in Fig. 3(*f*). The folding angle saturates after 100 s for currents 3 A and 2.8 A, after 200 s for 2.4 A, and after 400 s for 2.2 A. The maximum angles are 80, 78, 62, and 31 deg for currents 3 A, 2.8 A, 2.4 A, and 2.2 A. The folding was noticed to start in the opposite direction, then it returned back to the downward folding direction. This is shown as the negative values for the angle in the plots. The less current used for folding, the longer the observed negative folds.

3.2 Case 2. In this case, the same substrate configuration was investigated; however, the material used is NPS instead of PSPS. Sample was heated with the bottom tip of the resistive ribbon. The results of substrate folding are shown in Fig. 4. The schematic drawing of substrate folding is presented in Fig. 4(*a*). Results of folding angle as a function of time are shown in Figs. 4(*b*)–4(*d*) and 3(*e*) for currents 3 A, 2.8 A, 2.6 A, and 2.4 A, respectively. Figure 4(*f*) shows the average of the experimentally measured angles for different currents. The maximum angles are 46, 44, 38, and 28 deg for currents 3 A, 2.8 A, 2.6 A, and 2.4 A. Compared with PSPS case, the maximum angle for NPS is about 60% of the maximum angle for PSPS. Initial folding in the opposite direction is also observed for this case.

3.3 Case 3. In this case, the same substrate that was folded in case 1 was used, where a layer of Kapton tape is adhered to the

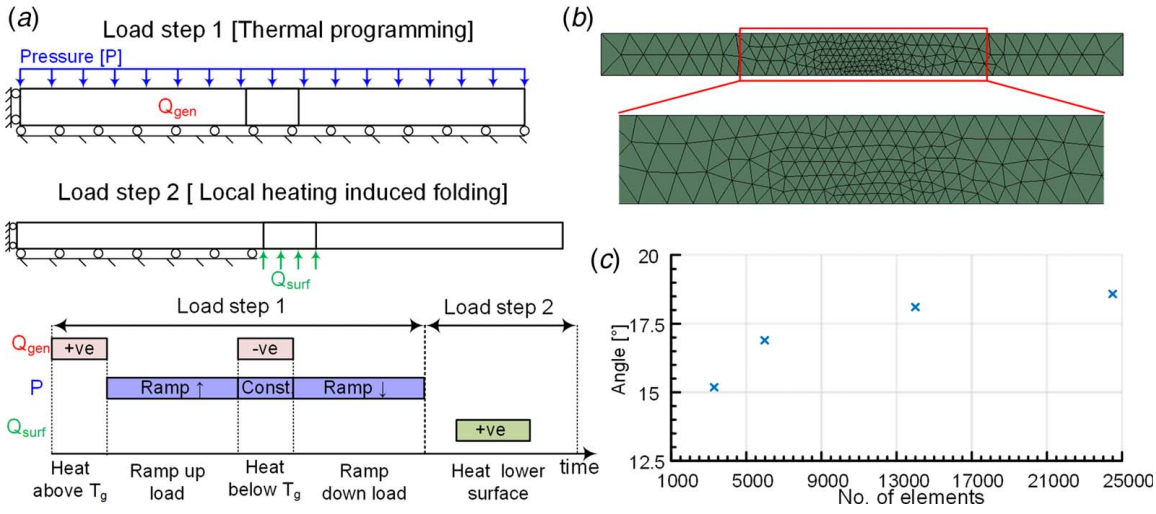

Fig. 2 (*a*) Loading and boundary conditions for the FEM, (*b*) tetrahedral mesh used for simulations, and (*c*) mesh convergence study showing steady-state folding angle at different element numbers

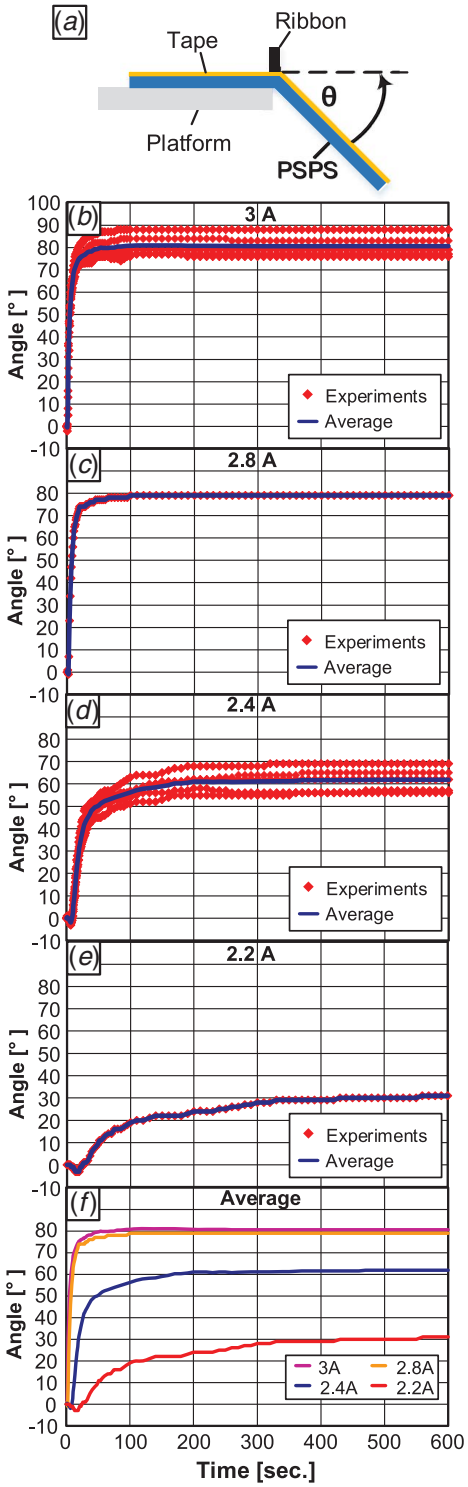

Fig. 3 Results for case 1: heating Kapton-covered PSPS by the bottom of the resistive ribbon for different currents: (*a*) schematic figure; (*b*–*e*) different currents: 3 A, 2.8 A, 2.4 A, and 2.2 A, respectively; and (*f*) comparison of the averages

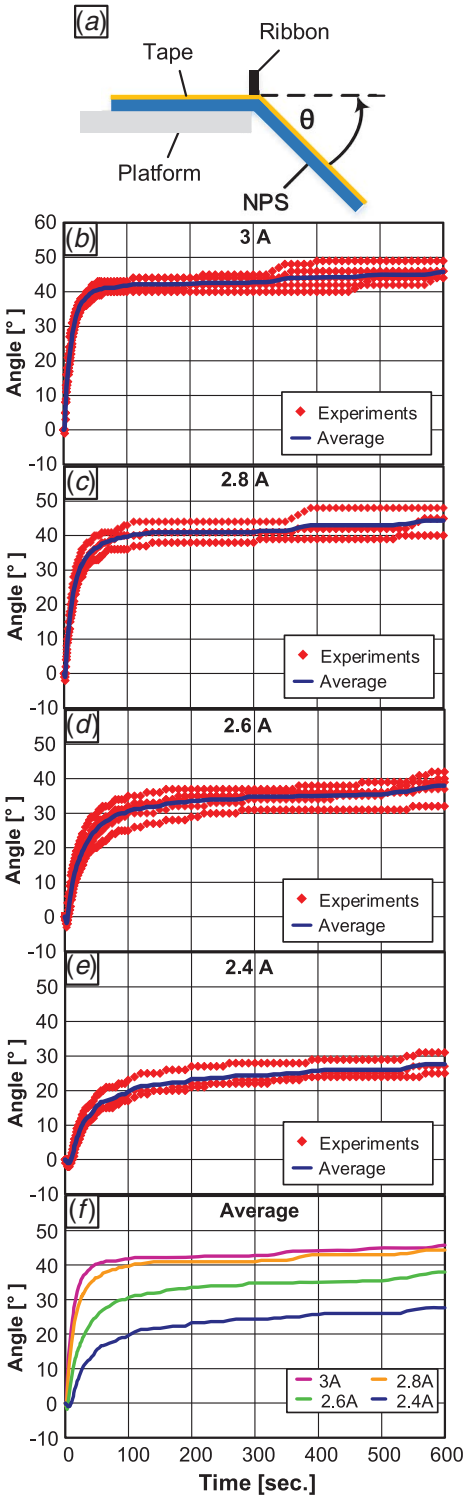

Fig. 4 Results for case 2: heating Kapton-covered NPS by the bottom of the resistive ribbon for different currents: (*a*) schematic; (*b*–*e*) different currents: 3 A, 2.8 A, 2.6 A, and 2.4 A, respectively; and (*f*) comparison of the averages

PSPS sheet. However, in case 3, the substrate is heated with the top tip of the resistive ribbon. The results of substrate folding are shown in Fig. 5. The schematic drawing of substrate folding is presented in Fig. 4(*a*). Results of folding angle as a function of time are shown in Figs. 5(*b*)–5(*f*) for currents 3 A, 2.8 A, 2.6 A, 2.4 A, and 2.2 A, respectively. The average of the experimentally measured angles is shown in each plot, and these averages are compared in Fig. 5(*g*). The folding angle saturates in the first 100 s for currents 3 A, 2.8 A, and 2.6 A, after 200 s for 2.4 A, and after 400 s for 2.2 A. The maximum angles are 87, 85, 69, 62, and 38 deg for currents 3 A, 2.8 A, 2.6 A, 2.4 A, and 2.2 A. It was observed that the maximum folding angle achieved by heating from tip top (case 3) is greater than the maximum folding angle achieved by heating from tip bottom (case 1) for PSPS. The initial folding in the opposite

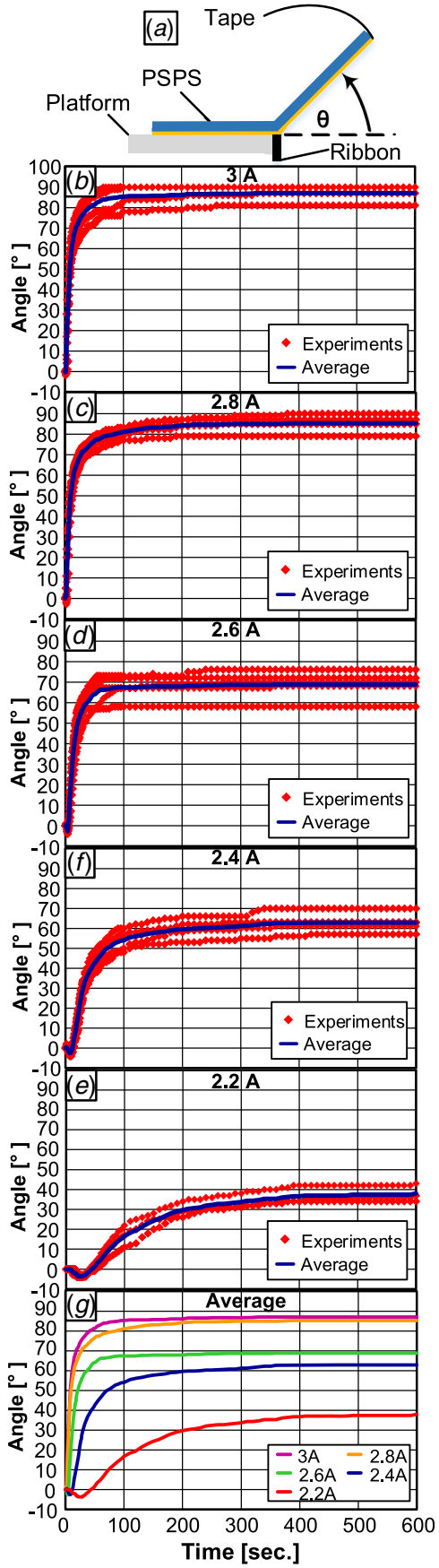

Fig. 5 Results for case 3: heating Kapton-covered PSPS by the top of the resistive ribbon for different currents: (*a*) schematic; (*b–f*) different currents: 3 A, 2.8 A, 2.6 A, 2.4 A, and 2.2 A, respectively; and (*g*) comparison of averages for each current

direction appeared in this case also, and it is more obvious in experiments with low currents.

3.4 Case 4. In this case, instead of PSPS, NPS was used with the Kapton polyimide tape with the same configuration of heating of case 3. The results of substrate folding are shown in Fig. 6. The schematic drawing of substrate folding is presented in Fig. 6(*a*). Results of folding angle as a function of time are shown in Figs. 6(*b*)–6(*f*) for currents 3 A, 2.8 A, 2.6 A, 2.4 A, and 2.2 A, respectively. In this experiment, the folding angle was found to be much lower than the other cases. The average of the experimentally measured angles is shown in each plot, and these averages are compared in Fig. 5(*g*). The folding angle saturates in the first 100 s for currents 3 A, 2.8 A, and 2.6 A, after 200 s for 2.4 A, and after 400 s for 2.2 A. The maximum folding angles are 12, 11, 9, 8, and 2 deg for currents 3 A, 2.8 A, 2.6 A, 2.4 A, and 2.2 A, respectively. Comparing these results with case 2, it can be concluded that the direction of heating could control the maximum folding angle which is an interesting aspect for achieving complex shapes. The initial folding in the opposite direction was also observed here. Most of the folding for 2.2 A current was in the negative direction.

3.5 Case 5. In this case, Kapton polyimide tape was used with direct contact between PSPS and the heating resistive ribbon. The PSPS contact was the top tip of the heating ribbon. The results of the bare substrate folding are shown in Fig. 7. The schematic drawing of substrate folding is presented in Fig. 7(*a*). Results of folding angle as a function of time are shown in Figs. 7(*b*)–7(*f*) for currents 3 A, 2.8 A, 2.6 A, 2.4 A, and 2.2 A, respectively. In these experiments, the material flows much faster which leads to excessive flow and possible melting of the PSPS. Some experiments failed due to problems in alignment between the PSPS and the heat ribbon. The average of the experimentally measured angles is shown in each plot, and these averages are collected in Fig. 7(*g*). The folding angle reaches 90 deg much faster in this case, and the experiments were stopped at this angle because of excessive material flow and melting after 90 deg angle. The polymer reaches 90 deg at 6, 7, 13, 18, and 60 s for currents 3 A, 2.8 A, 2.6 A, 2.4 A, and 2.2 A, respectively. The folding in the opposite direction did not appear in this case.

3.6 Case 6. In this case, the same substrate configuration as case 5 was utilized with NPS instead of PSPS. Also, the contact between NPS and heating ribbon was the top tip of the heating ribbon. The results for this case of bare NPS substrate folding are shown in Fig. 8. The schematic drawing of substrate folding is presented in Fig. 8(*a*). Results of folding angle as a function of time are shown in Figs. 8(*b*)–8(*f*) for currents 3 A, 2.8 A, 2.6 A, 2.4 A, and 2.2 A, respectively. The average of the experimentally measured angles is shown in each plot, and these averages are compared in Fig. 8(*g*). The folding angle reaches 90 deg for 3 A and 2.8 A currents after 36 and 120 s, respectively. The maximum folding angles are 86, 71, and 21 deg for currents 2.6 A, 2.4 A, and 2.2 A, respectively. The folding in the opposite direction did not appear in this case.

4 Discussion

After showing the results for different cases of self-folding in our study, they were juxtaposed in one figure to compare their dynamics. Figure 9 represents a summary for the folding results in all six cases. The figure shows the relation between the folding angle and the time on a log scale. Results show that PSPS folding has larger folding angles compared with NPS. This is explained by the relatively stronger forces from the shrinkage of SMPs [29], which is much more pronounced for the viscoelastic relaxation of prestrained samples (PSPS). The fastest self-folding occurred in case of bare PSPS due to the direct contact between the ribbon and

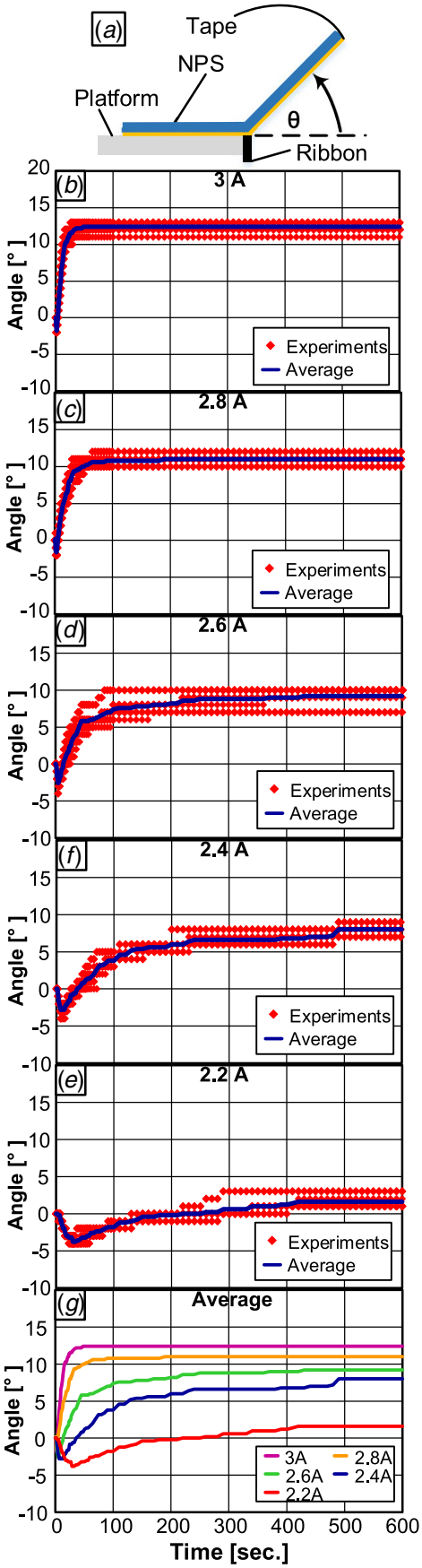

Fig. 6 Results for case 4: heating Kapton-covered NPS by the top of the ribbon for different currents: (*a*) schematic; (*b–f*) different currents: 3 A, 2.8 A, 2.6 A, 2.4 A, and 2.2 A, respectively; and (*g*) comparison of averages for each current

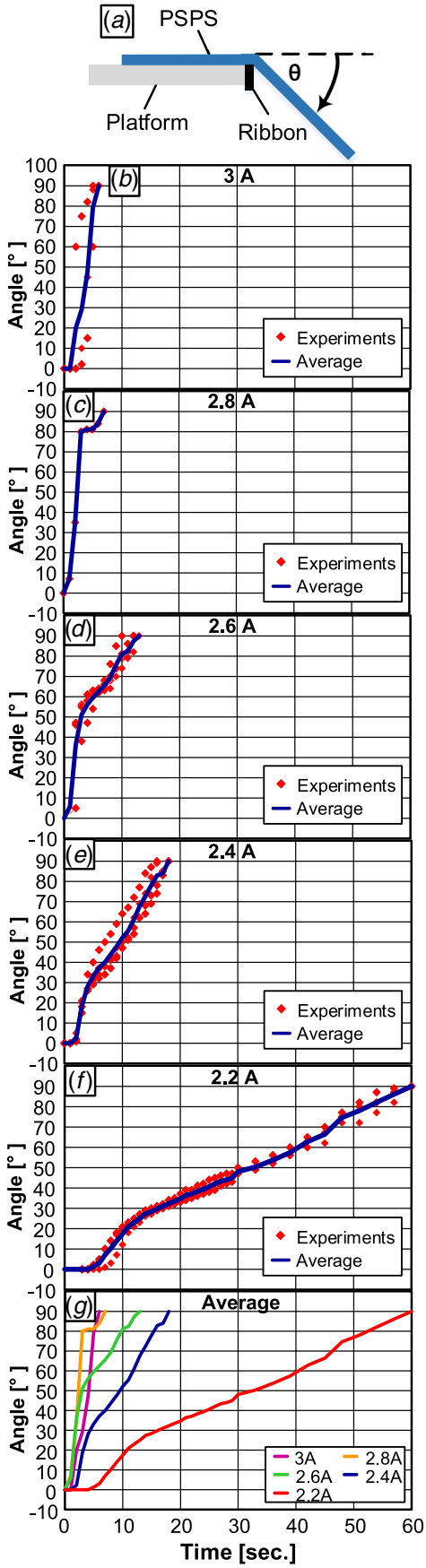

Fig. 7 Results for case 5: heating bare PSPS by the top of the resistive ribbon for different currents: (*a*) schematic; (*b–f*) different currents: 3 A, 2.8 A, 2.6 A, 2.4 A, and 2.2 A, respectively; and (*g*) comparison of averages for each current

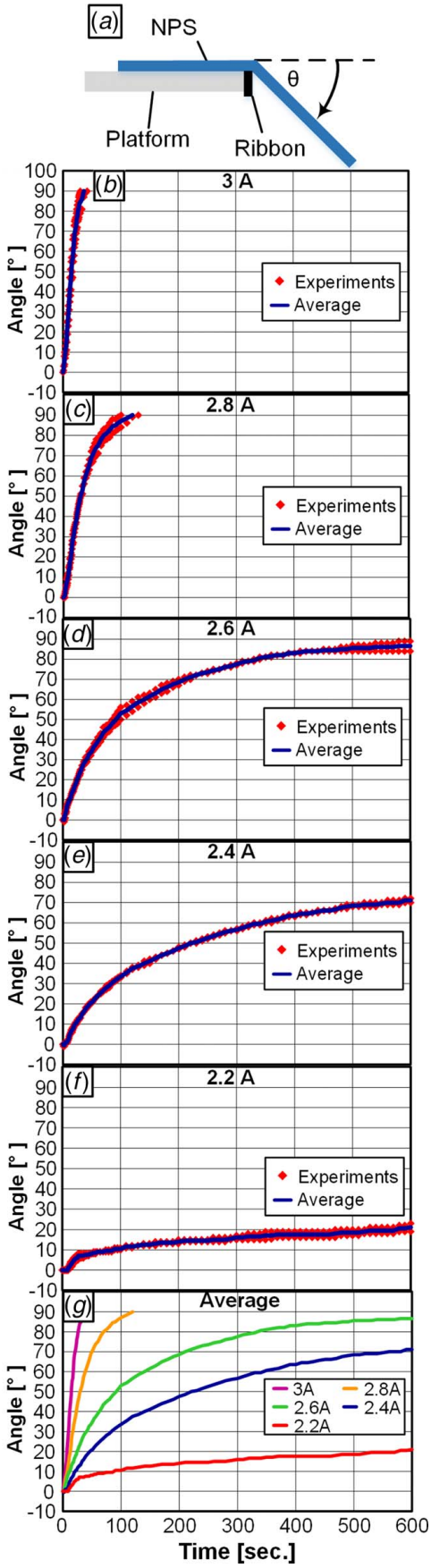

Fig. 8 Results for case 6: heating bare NPS by the top of the resistive ribbon for different currents: (*a*) schematic; (*b–f*) different currents: 3 A, 2.8 A, 2.6 A, 2.4 A, and 2.2 A, respectively; and (*g*) comparison of averages for each current

PSPS, which resulted in direct rapid heating, in contrast to the cases where the polyimide tape separated the heating ribbon and the sample.

Importantly, most of NPS cases did not reach 90 deg except in bare NPS. This result is explained based on the effect of gravity, which was previously shown to cause folding of non-SMP polymers [18]. In that case, the direct localized heating makes the material softer and deformable under small loads (in this case the weight of the overhung part of the sample). As can be seen from the summary results in Fig. 9(*f*), almost no folding is observed because the downward gravity force is counteracted by the upward folding resulting from the strain mismatch between the polystyrene sheet and the polyimide tape, as discussed below.

Another observation is that results for 3 A and 2.8 A currents are quite similar for the different cases, and this is attributed to the fact that for both cases, the temperatures (shown in Table 1) are well above the glass transition temperature. Tolley et al. have previously showed that the material transition from glassy to viscoelastic occurs linearly over a 30 °C temperature range around transition temperature [30]. Both temperatures are above the transition temperature (103 °C for polystyrene) with more than 15 °C.

We also observe that the cases with polyimide tape (cases 1–4) exhibit larger run-to-run variations (as observed from comparing multiple repeats in Figs. 3–6) than the last two cases (5 and 6) with no polyimide tape (as observed from comparing multiple repeats in Figs. 7 and 8). The variances for cases 1–4 were estimated to be three times as large that of cases 5 and 6 ($\sigma^2 = 9$ for cases 1–4; $\sigma^2 = 3$ for cases 5 and 6). This could be due to discrepancies in the method of adhering the polyimide tape to the polystyrene sheets. Small air gaps between the tape and the sheet can introduce variability in the heating that can explain the observed fold angle variations. Although we adopted a careful technique for applying the tape with a roller to minimize such air gaps, further research on developing an automated method for applying the tape may reduce these variations in the future.

4.1 Mechanism of Folding. We describe the main forces playing a significant role in the folding process, which are listed as follows:

(1) The shrinkage force resulting for the viscoelastic relaxation of the polymer. This force is only significant in the case of PSPS because it is pre-strained. On the other hand, this is not significant in the case of NPS, which is not pre-strained.
(2) The interfacial force resulting from the strain mismatch between the polystyrene film and the polyimide tape (in cases where tape was used). This force is also more significant in the cases of PSPS because the shrinkage resulting from the viscoelastic relaxation of pre-strained polymers is much more significant than the shrinkage of NPS.
(3) The downward gravity force acting on the overhung part of the sample, which is much smaller than the previous two forces in the cases of PSPS, and hence can be neglected in those cases. On the other hand, it is significant in the case of NPS, where no appreciable shrinkage takes place.

Figure 10 schematically illustrates the above-mentioned forces acting on the substrate in each case. Figure 10(*a*) shows cases 1 and 2, where the substrate has the polyimide layer, and it is heated by the bottom tip of the heating ribbon. Figure 10(*b*) shows cases 3 and 4, where the substrate has the polyimide layer, and it is heated by the top tip of the heating ribbon. Figure 10(*c*) shows cases 5 and 6, where the polymer is bare, and it is heated by the top tip of the heating ribbon.

The shrinkage force is induced due to the gradient temperature through the sheet thickness, which produce gradient shrinkage. This variation of shrinkage through thickness produces a moment that causes the folding. Gravity forces become significant when local heating compromises the bending stiffness of the sample at the line of contact with the ribbon, i.e., when the polymer

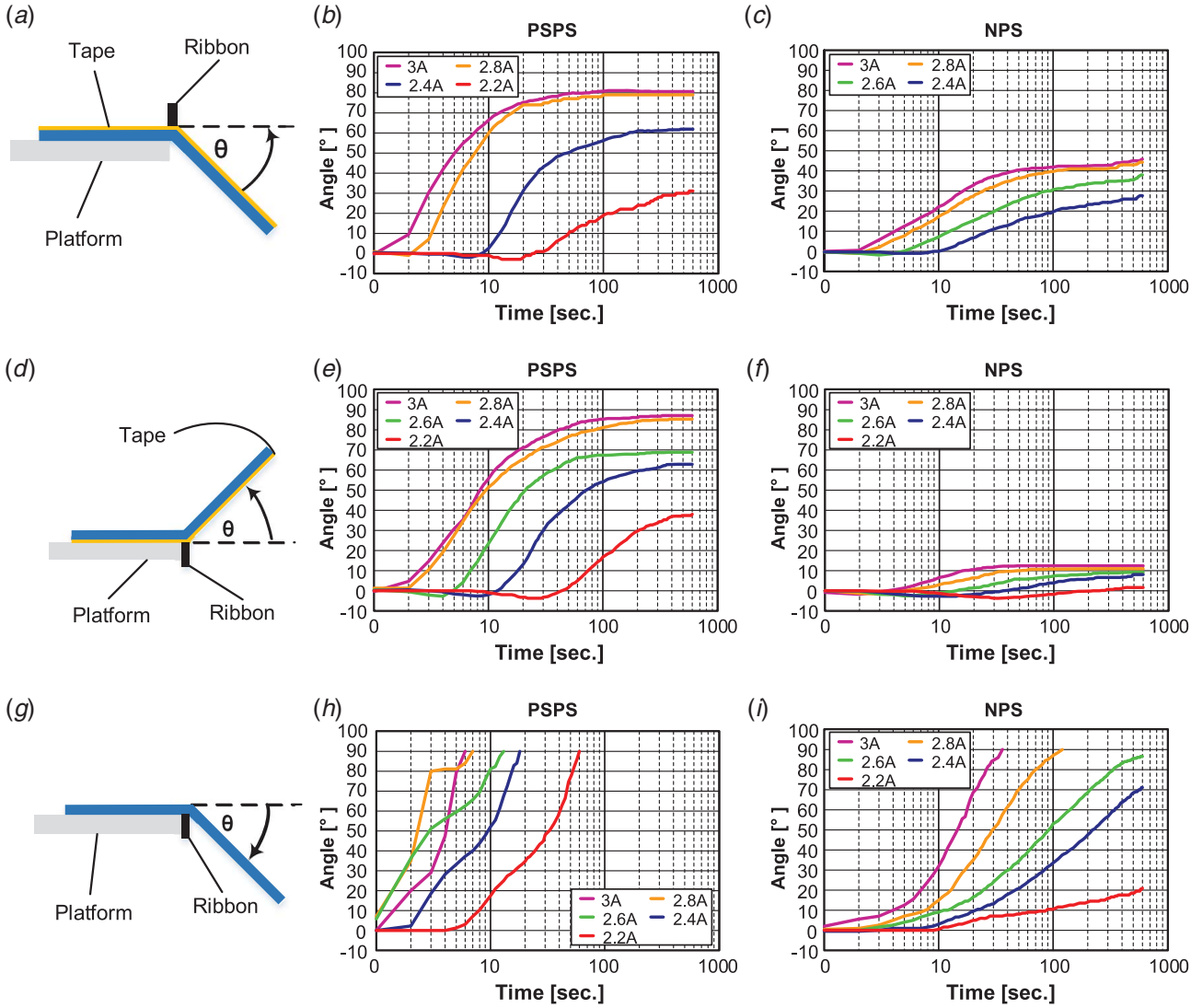

Fig. 9 Summary for the folding results for different configurations and currents: (*a*, *d*, *g*) schematics for each case; (*b* and *c*) comparing the current-dependent folding for Kapton-covered samples, heated by the bottom of the ribbon for PSPS (case 1) and NPS (case 2), respectively; (*e* and *f*) comparing the current-dependent folding for Kapton-covered samples, heated by the top of the ribbon for PSPS (case 3) and NPS (case 4), respectively; and (*b* and *c*) comparing the current-dependent folding for bare samples, heated by the top of the ribbon for PSPS (case 5) and NPS (case 6), respectively

temperature locally increases, its stiffness locally decreases, which makes the polymer softer at the line of heating. Consequently, the polymer starts to fold in the direction of gravity, and this mechanism is only significant in NPS cases and is not significant in other PSPS cases, where other dominant forces, such as shrinkage and mismatch of straining between the substrate and the polyimide tape, are much stronger. In case 2 (Fig. 9(*c*)), both gravity and the interfacial mismatch forces act in the same downward folding direction, and this is why significant folding angles up to 40 deg can be achieved even though this polymer is not pre-strained. On the other hand, in case 4 (Fig. 9(*f*)), gravity and the interfacial mismatch forces act in opposing directions, which explains the very small folding angles achieved (less than 10 deg).

The interfacial strain mismatch or bimaterial effect that we observe in the cases of using the polyimide tape on the substrate (cases 1–4) is important because it uniquely enables bidirectional

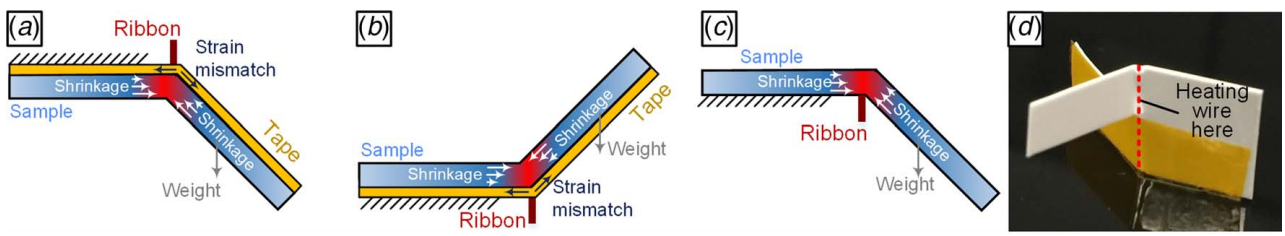

Fig. 10 Schematic for the mechanism of bidirectional folding: (*a* and *b*) strain mismatch is dominant over gradient shrinkage or weight and (c) gradient shrinkage is dominant in case of SMP, and weight is only significant in case of non-SMP material

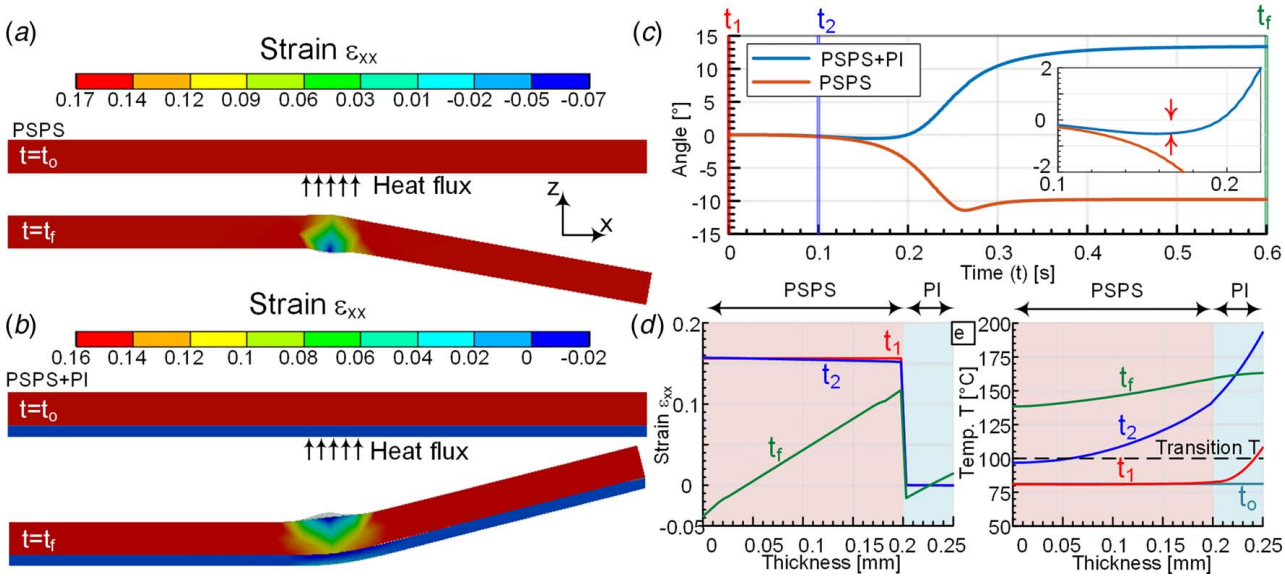

Fig. 11 Finite element modeling of PSPS and PI + PSPS case: (*a*) axial strain contours before and after introducing heat to a PSPS sheet, (*b*) axial strain contours before and after introducing heat to a PSPS sheet with a polyimide layer, (*c*) change of folding angle with time for the cases presented in (*a* and *b*) with inset at time 0.1–0.2 s, and (*d* and *e*) axial strain and temperature across the thickness of the PSPS sheet with polyimide illustrating the change during different points of heating

folding using a single heating ribbon. Figure 10(*d*) shows an experimental result for bidirectional folding on the same sample using a Kapton-covered PSPS sheet, where one side had tape and the other was without tape. These unprecedented results highlight the capabilities of our approach as a promising route in manufacturing complex 3D shapes that have hollow lightweight structure and smooth surfaces. The smoothness of the surface is a significant distinguishing factor of this approach for manufacturing 3D polymeric structures, when compared with polymer 3D printing methods, such as fused deposition modeling (FDM) or stereolithography (SLA). While the 3D geometries that can be achieved by folding is limited compared with 3D printing methods, the fast speed and surface properties make folding an attractive alternative. Another advantage of folding-based methods is the low cost of the 2D polymer sheets used, including the low shipping cost resulting from the ease of packing and handling stacked sheets.

4.2 Finite Element Model Results. The FEM results match the experimental observations of cases 3 and 5 where in the case without polyimide the sheet folded downwards and in the case with polyimide it folded upwards (the opposite direction) as shown in Figs. 11(*a*) and 11(*b*).

Additionally, the initial folding in the bilayer cases matches what was observed where it initially folds downward and then reverses direction with time as observed in Fig. 11(*c*) (see the arrow pointing to negative angles in the inset). Examining the thermal and axial strain results explains the bidirectional folding phenomenon as shown in Figs. 11(*d*) and 11(*e*). Initially at t_1, the temperature across the thickness is mostly lower than the transition, hence no change in the strain is observed. At t_2, the temperature across the thickness is mostly above the transition temperature, with the higher temperature being toward the polyimide side. This leads to a small shrinkage on the polyimide side but due to the temperature depended relaxation rates, does not reflect yet on the no polyimide side. This leads to a small-angle fold downwards (Fig. 11(*c*)) which was also observed in experiments (Fig. 9(*e*)). Eventually, the no polyimide side shrinks more than the polyimide side, which is constrained from shrinkage by the interface with polyimide tape (under slight compressive axial strain at t_f). This leads to the upward folding at t_f observed both in the simulation and experimentally.

Taken together our results show that the ability to control the speed and direction of folding based on electric current control is promising for application in a scaled manufacturing setting, where precise folds could be achieved by controlling the temperature and timing of heating in a preprogrammed spatiotemporal distribution. For that purpose, a designed 2D pattern of resistively heated wires or ribbons could be placed on the polymer sheet in order to direct local folding. Moreover, the approach of directed self-folding based on localized heating can be combined with modern cybermanufacturing infrastructure in order to achieve mass customization in 3D fabrication at on-demand stations or kiosks [4,5].

5 Conclusion

Current-controlled resistive heating is an attractive approach for local activation of self-folding in shape memory polymers. Real-time measurements of folding dynamics were recorded for different configurations having a variation of materials and heating direction (top and bottom heating). Also, we investigated the effect of using a polyimide tape (Kapton) on folding kinetics and direction, compared with the bare samples. Higher currents create much faster folds with more material flow. For PSPS, using the polyimide tape on one side controls fold direction with respect to the heating ribbon. For NPS, gravity dominates in the absence of tape and determines the direction of folding. By using different configurations, bidirectional folding can be achieved. Future work will include larger samples with more complex arrangements of geometrically and physically different heating ribbons/wires for sequential folding with different angles and directions, in order to achieve origami-based manufacturing of 3D polymer objects. Challenges will include setting the proper wiring arrangement to reflect a complex design, managing the sequence of heating, and the proper placement of the second layer to utilize the bidirectional folding effectively.

Acknowledgment

This research was supported in part by the National Science Foundation (NSF) under Award No. 2028580 (any opinions, findings, and conclusions or recommendations expressed in this material are those of the author(s) and do not necessarily reflect the

views of the National Science Foundation). This work was also funded by the Department of Industrial Engineering at the University of Pittsburgh. E. Poska was supported by the PPG Foundation Fellowship through the Swanson School of Engineering Undergraduate Research Program.

Conflict of Interest

There are no conflicts of interest.

Data Availability Statement

The datasets generated and supporting the findings of this article are obtainable from the corresponding author upon reasonable request. The authors attest that all data for this study are included in the paper.

References

[1] Tolley, M. T., Felton, S. M., Miyashita, S., Xu, L., Shin, B., Zhou, M., Rus, D., and Wood, R. J., 2013, "Self-Folding Shape Memory Laminates for Automated Fabrication," IEEE International Conference on Intelligent Robots and Systems, Tokyo, Japan.
[2] Turner, N., Goodwine, B., and Sen, M., 2016, "A Review of Origami Applications in Mechanical Engineering," Proc. Inst. Mech. Eng. Part C J. Mech. Eng. Sci., **230**(14), pp. 2345–2362.
[3] Liu, Z., Cui, A., Li, J., and Gu, C., 2019, "Folding 2D Structures Into 3D Configurations at the Micro/Nanoscale: Principles, Techniques, and Applications," Adv. Mater., **31**(4), pp. 1–20.
[4] Wang, Z., Iquebal, A. S., and Bukkapatnam, S. T. S., 2018, "A Vision-Based Monitoring Approach for Real-Time Control of Laser Origami Cybermanufacturing Processes," Procedia Manuf., **26**, pp. 1307–1317.
[5] Iquebal, A. S., Wang, Z., Ko, W. H., Wang, Z., Kumar, P. R., Srinivasa, A., and Bukkapatnam, S. T. S., 2018, "Towards Realizing Cybermanufacturing Kiosks: Quality Assurance Challenges and Opportunities," Procedia Manuf., **26**, pp. 1296–1306.
[6] Leong, T. G., Zarafshar, A. M., and Gracias, D. H., 2010, "Three-Dimensional Fabrication at Small Size Scales," Small, **6**(7), pp. 792–806.
[7] Liu, Y., Genzer, J., and Dickey, M. D., 2016, "'2D or Not 2D': Shape-Programming Polymer Sheets," Prog. Polym. Sci., **52**, pp. 79–106.
[8] Hawkes, E., An, B., Benbernou, N. M., Tanaka, H., Kim, S., Demaine, E. D., Rus, D., and Wood, R. J., 2010, "Programmable Matter by Folding," Proc. Natl. Acad. Sci. U. S. A., **107**(28), pp. 12441–12445.
[9] Ilievski, F., Mazzeo, A. D., Shepherd, R. F., Chen, X., and Whitesides, G. M., 2011, "Soft Robotics for Chemists," Angew. Chemie—Int. Ed., **50**(8), pp. 1890–1895.
[10] Small, W. IV, Singhal, P., Wilson, T. S., and Maitland, D. J., 2010, "Biomedical Applications of Thermally Activated Shape Memory Polymers," J. Mater. Chem., **20**(17), pp. 3356–3366.
[11] Yakacki, C. M., Shandas, R., Lanning, C., Rech, B., Eckstein, A., and Gall, K., 2007, "Unconstrained Recovery Characterization of Shape-Memory Polymer Networks for Cardiovascular Applications," Biomaterials, **28**(14), pp. 2255–2263.
[12] Zirbel, S. A., Trease, B. P., Magleby, S. P., and Howell, L. L., 2014, "Deployment Methods for an Origami-Inspired Rigid-Foldable Array," Proceedings of the 42nd Aerospace Mechanisms Symposium, Baltimore, MD.
[13] Guo, X., Li, H., Ahn, B. Y., Duoss, E. B., Hsia, K. J., Lewis, J. A., and Nuzzo, R. G., 2009, "Two- and Three-Dimensional Folding of Thin Film Single-Crystalline Silicon for Photovoltaic Power Applications," Proc. Natl. Acad. Sci. U. S. A., **106**(48), pp. 20149–20154.
[14] Cho, J. H., Hu, S., and Gracias, D. H., 2008, "Self-Assembly of Orthogonal Three-Axis Sensors," Appl. Phys. Lett., **93**(4), pp. 1–4.
[15] Judy, J. W., and Muller, R. S., 1997, "Magnetically Actuated, Addressable Microstructures," J. Microelectromech. Syst., **6**(3), pp. 249–255.
[16] Yi, Y. W., and Liu, C., 1999, "Magnetic Actuation of Hinged Microstructures," J. Microelectromech. Syst., **8**(1), pp. 10–17.
[17] Martinez, R. V., Fish, C. R., Chen, X., and Whitesides, G. M., 2012, "Elastomeric Origami: Programmable Paper-Elastomer Composites as Pneumatic Actuators," Adv. Funct. Mater., **22**(7), pp. 1376–1384.
[18] Kusuda, S., Sawano, S., and Konishi, S., 2007, "Fluid-Resistive Bending Sensor Having Perfect Compatibility With Flexible Pneumatic Balloon Actuator," 2007 IEEE 20th International Conference on Micro Electro Mechanical Systems, Hyogo, Japan.
[19] Guan, J., He, H., Hansford, D. J., and Lee, L. J., 2005, "Self-Folding of Three-Dimensional Hydrogel Microstructures," J. Phys. Chem. B, **109**(49), pp. 23134–23137.
[20] Stoychev, G., Puretskiy, N., and Ionov, L., 2011, "Self-Folding All-Polymer Thermoresponsive Microcapsules," Soft Matter, **7**(7), p. 3277.
[21] Luo, J. K., Huang, R., He, J. H., Fu, Y. Q., Flewitt, A. J., Spearing, S. M., Fleck, N. A., and Milne, W. I., 2006, "Modelling and Fabrication of Low Operation Temperature Microcages With a Polymer/Metal/DLC Trilayer Structure," Sens. Actuators A Phys., **132**(1 SPEC. ISS.), pp. 346–353.
[22] Suzuki, K., Yamada, H., Miura, H., and Takanobu, H., 2007, "Self-Assembly of Three Dimensional Micro Mechanisms Using Thermal Shrinkage of Polyimide," Microsyst. Technol., **13**(8–10), pp. 1047–1053.
[23] Mueller, S., Kruck, B., and Baudisch, P., 2013, "LaserOrigami," CHI '13 Extended Abstracts on Human Factors in Computing Systems, Paris, France.
[24] Cho, J. H., Azam, A., and Gracias, D. H., 2010, "Three Dimensional Nanofabrication Using Surface Forces," Langmuir, **26**(21), pp. 16534–16539.
[25] Liu, Y., Boyles, J. K., Genzer, J., and Dickey, M. D., 2012, "Self-Folding of Polymer Sheets Using Local Light Absorption," Soft Matter, **8**(6), pp. 1764–1769.
[26] Zhang, Q., Wommer, J., O'Rourke, C., Teitelman, J., Tang, Y., Robison, J., Lin, G., and Yin, J., 2017, "Origami and Kirigami Inspired Self-Folding for Programming Three-Dimensional Shape Shifting of Polymer Sheets With Light," Extrem. Mech. Lett., **11**, pp. 111–120.
[27] Davis, D., Mailen, R., Genzer, J., and Dickey, M. D., 2015, "Self-Folding of Polymer Sheets Using Microwaves and Graphene Ink," RSC Adv., **5**(108), pp. 89254–89261.
[28] Felton, S. M., Tolley, M. T., Shin, B., Onal, C. D., Demaine, E. D., Rus, D., and Wood, R. J., 2013, "Self-Folding With Shape Memory Composites," Soft Matter, **9**(32), pp. 7688–7694.
[29] Felton, S., Tolley, M., Demaine, E., Rus, D., and Wood, R., 2014, "A Method for Building Self-Folding Machines," Science, **345**(6197), pp. 644–646.
[30] Tolley, M. T., Felton, S. M., Miyashita, S., Aukes, D., Rus, D., and Wood, R. J., 2014, "Self-Folding Origami: Shape Memory Composites Activated by Uniform Heating," Smart Mater. Struct., **23**(9), p. 094006.
[31] An, B., Miyashita, S., Tolley, M. T., Aukes, D. M., Meeker, L., Demaine, E. D., Demaine, M. L., Wood, R. J., and Rus, D., 2014, "An End-to-End Approach to Making Self-Folded 3D Surface Shapes by Uniform Heating," IEEE International Conference on Robotics & Automation, Hong Kong, China.
[32] Liu, Y., Miskiewicz, M., Escuti, M. J., Genzer, J., and Dickey, M. D., 2014, "Three-Dimensional Folding of Pre-Strained Polymer Sheets via Absorption of Laser Light," J. Appl. Phys., **115**(20), p. 204911-1.
[33] Piqué, A., Mathews, S., Birnbaum, A., and Charipar, N., 2011, "Microfabricating 3D Structures by Laser Origami," SPIE Newsroom, Bellingham WA.
[34] ANSYS, 2011, *Mechanical APDL Element Reference*, ANSYS, Inc.
[35] Mailen, R. W., Liu, Y., Dickey, M. D., Zikry, M., and Genzer, J., 2015, "Modelling of Shape Memory Polymer Sheets That Self-Fold in Response to Localized Heating," Soft Matter, **11**(39), pp. 7827–7834.
[36] Mailen, R. W., Dickey, M. D., Genzer, J., and Zikry, M. A., 2017, "A Fully Coupled Thermo-Viscoelastic Finite Element Model for Self-Folding Shape Memory Polymer Sheets," J. Polym. Sci. Part B Polym. Phys., **55**(16), pp. 1207–1219.